

PAPER

Effect of polydispersity in concentrated magnetorheological fluids

To cite this article: Júlio Gabriel de Falco Manuel *et al* 2023 *Smart Mater. Struct.* **32** 045014

View the [article online](#) for updates and enhancements.

You may also like

- [The effects of polydispersity on the initial susceptibilities of ferrofluids](#)
Philip J Camp, Ekaterina A Elfimova and Alexey O Ivanov
- [Hard-body models of bulk liquid crystals](#)
Luis Mederos, Enrique Velasco and Yuri Martínez-Ratón
- [Crystallization kinetics of colloidal model suspensions: recent achievements and new perspectives](#)
Thomas Palberg

Effect of polydispersity in concentrated magnetorheological fluids

Júlio Gabriel de Falco Manuel¹ , Antonio José Faria Bombard^{1,*}  and Eric R Weeks² 

¹ Physics and Chemistry Institute - IFQ, Federal University of Itajubá - UNIFEI, Itajubá, MG 37.500-903, Brazil

² Department of Physics, Emory University, Atlanta, GA 30322, United States of America

E-mail: antonio.bombard@gmail.com

Received 24 May 2022, revised 13 December 2022

Accepted for publication 8 February 2023

Published 14 March 2023



CrossMark

Abstract

Magnetorheological fluids (MRF) are smart materials of increasing interest due to their great versatility in mechanical and mechatronic systems. As main rheological features, MRFs must present low viscosity in the absence of magnetic field (0.1–1.0 Pa.s) and high yield stress (50–100 kPa) when magnetized, in order to optimize the magnetorheological effect. Such properties, in turn, are directly influenced by the composition, volume fraction, size, and size distribution (polydispersity) of the particles, the latter being an important piece in the improvement of these main properties. In this context, the present work aims to analyze, through experiments and simulations, the influence of polydispersity on the maximum packing fraction, on the yield stress under field (on-state) and on the plastic viscosity in the absence of field (off-state) of concentrated MRF ($\phi = 48.5$ vol.%). Three blends of carbonyl iron powder (CIP) in polyalphaolefin oil were prepared. These blends have the same mode, but different polydispersity indexes (α), ranging from 0.46 to 1.44. Separate simulations show that the random close packing fraction increases from about 68% to 80% as the polydispersity indexes increase over this range. The on-state yield stress, in turn, is raised from 30 ± 0.5 kPa to 42 ± 2 kPa ($B \approx 0.57$ T) and the off-state plastic viscosity, is reduced from 4.8 Pa.s to 0.5 Pa.s. Widening the size distributions, as is well known in the literature, increases packing efficiency and reduces the viscosity of concentrated dispersions, but beyond that, it proved to be a viable way to increase the magnetorheological effect of concentrated MRF. The Brouwers model, which considers the void fraction in suspensions of particles with lognormal distribution, was proposed as a possible hypothesis to explain the increase in yield stress under magnetic field.

Supplementary material for this article is available [online](#)

Keywords: magnetorheological fluids, polydispersity, yield stress, plastic viscosity, size mixtures, packing simulations

(Some figures may appear in colour only in the online journal)

1. Introduction

In 1948, at the US National Bureau of Standards, Jacob Rabinow described a magnetizable fluid with tunable rheological properties, creating a completely new field of study for both rheology and rheometry: magnetorheology [1].

Magnetorheological fluids (MRF) stand out as a type of smart materials that, when exposed to an external magnetic field, undergo a rapid and reversible transition from the liquid state to a quasi-solid state, modifying important rheological properties, such as viscoelasticity, plastic viscosity, yield stress, among others [2–4].

Such transition, the so-called magnetorheological effect [5], makes MRF extremely versatile materials, especially in mechanical systems that need vibration or torque control, such

* Author to whom any correspondence should be addressed.

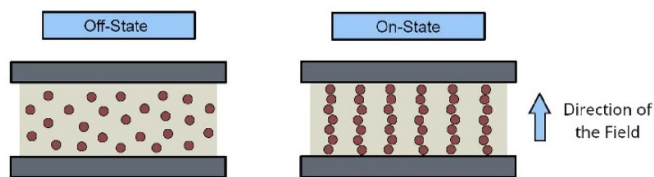


Figure 1. The magnetorheological effect, where the imposed magnetic field is vertical (parallel to the chains of particles) in the right-side image.

as dampers, brakes, and clutches [2, 6]. In addition, recent research indicates that MRF are also viable options in high-precision polishing [7], robotics [8] (mechatronics), and even in the construction of devices for biomedical applications such as actuators in upper limb rehabilitation [9] and novel hydraulic actuation systems in surgeries [10].

This versatility is directly linked to the practicality of the magnetorheological effect: the magnetization of the suspended particles allows one to easily control the material's viscosity. With the application of an external magnetic field, each iron particle quickly becomes a dipole, interacting with adjacent ones. Such attractive interactions generate chain-like structures, aligned in the direction of the field, as illustrated in figure 1 [2, 3, 5, 11].

These structures create resistance to flow, strengthening the suspension and, effectively, increasing its viscosity. Furthermore, the ability of these chain-like structures to withstand—to a certain extent—applied stresses is an extremely important factor for the applicability of MRFs in mechanical systems. It is also worth mentioning that the strength of these structures is strictly related to the magnitude of the dipolar interactions, which is influenced by the magnetic field strength, concentration, magnetic properties, and shape of the utilized particles [3, 5, 12].

The composition of MRF is characterized by simplicity: there is a dispersed solid phase, in the form of magnetizable particles (typically up to 50% of the volume), with a usual size of 0.1–10 μm and a carrier liquid. For solid-phase formulation, ferrimagnetic materials (magnetite and chromium dioxide) and ferromagnetic materials (iron and carbonyl iron powder) can be used, with carbonyl iron powder being the most common choice due to its high saturation magnetization. As for the carrier liquid, typical options include mineral or vegetable oils, synthetic or silicone oils, polyesters, polyethers, hydrocarbons, water, and ionic liquids [2, 11, 13, 14]. The liquid must have a wide operable temperature range [6] (–40 to +150 $^{\circ}\text{C}$, at least), be chemically inert (non-corrosive and non-reactive) in relation to the iron powder and other materials, and, preferably, be non-toxic.

To avoid agglomeration and sedimentation of the suspended particles, as well as controlling viscosity, many patents also include surfactants and thixotropic additives in their composition. It is clear, therefore, that the formulation of a MRF is extremely dependent on the desired applications [3, 6, 11, 13].

Over the last few decades, much research has been carried out to improve the quality of the prepared MRF, as well as to

optimize the magnetorheological effect under different conditions. As ideal properties, a MRF should have low viscosity in the absence of field (off-state), high viscosity in the presence of field (on-state), and high yield stress, when magnetized [2, 3, 12, 15].

In this context, many studies indicate that size and size distribution of particles are important factors in the manipulation of these properties [4, 12, 15]. It is well established in the literature that the viscosity of concentrated suspensions or emulsions can be significantly reduced by employing mixtures of particle sizes, be they bidisperse, tridisperse, or even polydisperse. Based on this, two parameters are key: (a) the ratio of particle sizes, and (b) the proportion in quantity between classes of a given size. In the case of dispersions where the suspended phase has the same modal (or median) size, it is also widely recognized that the broader the size distribution used, the lower the viscosity of the suspension for the same volume fraction [16–19].

However, for most suspensions, including electrorheological fluids (ERF) and MRF, this effect is only evident in fractions well above 20 vol%, and the more concentrated the suspension, the more pronounced the effect is. With that in mind, the advantage of using polydisperse mixtures in the development of these fluids should be clear: as the MR or ER effect under field increases with the volume fraction, the more concentrated the fluid, the greater yield stress will be, under an applied field. On the other hand, it is also known that the viscosity of any dispersion increases dramatically with the volume fraction and this effect is even more pronounced with the use of finer particles. Therefore, one must carefully adjust the particle size distribution (PSD) as, in the absence of an applied field, the viscosity should be as low as possible, to maximize the MR effect. For the on-field yield stress, however, it is still controversial whether there is an advantage in using distributions with a wide range of sizes (high values of standard deviation or polydispersity indexes — α).

In this context, this work aims to demonstrate how blends of particles with the same mode, but different degrees of polydispersity, allow one to obtain MRF with greater random close packing, larger on-state yield stresses, and lower off-state viscosities. At first, a literature review is performed, followed by a brief discussion about PSDs. Then, the methodology of the experiments and simulations are given, succeeded by a discussion of the results. Finally, the work is concluded and proposals for future research are presented.

2. Literature review

In the literature, numerous studies indicate that size and size distribution of particles are important factors to control the central properties of MRF. However, an in-depth analysis of the published papers reveals that these results are, for the most part, conflicting and, therefore, a recap of their main conclusions is necessary.

Among these papers, Ota and Miyamoto [19], working with simulations of cubic particles with only two sizes (size ratios = 1:1, 1:2, 2:3, 3:4 and 4:5) in ERF with $\phi = 20$

vol%, concluded that: ‘...the ERF consisting of only the same particles gives the largest static yield stress.’. In this case, however, in addition to not presenting experimental results and the particle concentration being moderate, the effect of continuous polydispersity was not included in the simulations.

Lemaire *et al* [20] experimentally investigated, in a stress-controlled rheometer with parallel plates and modified to apply magnetic fields, two magnetorheological systems: one based on polystyrene microspheres with magnetite inclusions, dispersed in water, and another based on dispersed glass microspheres in an aqueous ferrofluid. This material, called an inverse ferrofluid (IFF), consists of a dispersion of non-magnetic micrometric particles in a ferrofluid [21]. In the first case, polydisperse particles in a volumetric concentration of only 5 vol% were used, and, in the second case, almost monodisperse ($45 \pm 5 \mu\text{m}$) and polydisperse (5–50 μm) glass spheres were compared, in a concentration $\phi = 20 \text{ vol\%}$. The applied magnetic field was modest: only 750 Oe ($H \approx 60 \text{ kA m}^{-1}$). In this context, the authors stated: ‘For a field $H = 750 \text{ Oe}$, the difference between the monodisperse and the polydisperse samples is not detectable within the precision of our measurements.’.

Wang *et al* [22] evaluated, through simulations, ER fluids prepared with three volume fractions: 16 vol%, 24 vol%, and 31 vol%. Assuming a normal (Gaussian) distribution for the particles, with a standard deviation σ in the range of 0–3.0, the authors concluded that: ‘The shear stress of the fluid is found to decrease with the increase of the variance σ^2 of the Gaussian distribution of particle sizes.’. From figure 2 of their work, it is clearly seen that the monodisperse particles show the highest values of shear stress.

Similar to Wang’s work, but assuming only monodisperse particles with two different sizes, Mori *et al* [23] evaluated, through simulations, ER fluids with concentrations of 11 vol%, 20 vol%, and 30 vol%. In this scenario, the particles had a diameter of 1.9 or 3.8 μm (size ratio 1:2) and the authors concluded that: ‘A computer simulation based on a point dipole approximation for the interaction between particles was carried out. When small and large particles, with a diameter ratio of 1:2, were mixed in equal numbers of particles, chain-like clusters consisting of both sizes of particles were formed. The shear stress and the response time of the binary size system were close to those of the uniform size system when the total volume fraction of particles was kept constant.’.

de Gans *et al* [24], in turn, experimentally studied dispersions of silica nanoparticles in a ferrofluid (IFF), in two concentrations: $\phi = 5.7 \text{ vol\%}$ and 18 vol%. In this context, the nanoparticles had average radius sizes of 53 nm, 84 nm, 138 nm, or 189 nm and, in addition to studying the effects of particle size, the authors also mention the so-called ‘size variance’. However, the technique used to obtain the silica particles (Stöber method) is well known for generating almost perfect monodisperse particles, with size variations so small that they can be considered negligible. The authors, therefore, conclude that: ‘...Our measurements indicate that the influence of particle size on $G'(\omega)$ and $\eta(\dot{\gamma})$ is very weak if there is any. These measurements were not accurate enough to give decisive information on the influence of the polydispersity on the

rheological properties, but they suggest that $G'(\omega)$ and $\eta(\dot{\gamma})$ decrease with increasing polydispersity.’.

See *et al* [25], in turn, investigated the effect of mixtures of different particle sizes on the response of electrorheological fluids based on sulfonated polystyrene-co-divinyl benzene (ion exchange resin) and silicone oil, in uniform shear flow. By using particles with sizes of 15 μm and 50 μm , the authors claimed that: ‘The concentration in both systems was 10 wt%, and the particles were spherical in shape and highly monodisperse, which was also confirmed by microscopic observation.’. Considering the typical density values of these materials and the concentration of 10% by mass, a volumetric fraction $\phi \sim 7.6 \text{ vol\%}$ can be inferred. This study, therefore, focused on bidisperse ERFs with a particle size ratio of 3:10. However, as in the study from de Gans, nothing can be inferred about the effect of the width of a unimodal distribution. The authors also stated: ‘...the highest electrorheological effect occurred with a 50:50 mixed suspension of small and large particles...’ and, further, that: ‘The polydispersity of particle sizes clearly influences the electrorheological response of optimal ER materials.’. However, as already mentioned, this system is bimodal and, therefore, different from a unimodal distribution with a high standard deviation.

Trendler and Böse [26] studied, experimentally, MRF prepared through mixtures of carbonyl iron particles whose size distribution is log-normal. Fine particles, with an average size of 1.8 μm , and coarse particles, with an average size of 6.8 μm , were used during preparation. In this case, unlike See *et al* (2002), the authors utilized two size distributions with equal dispersity, that is, $\text{Span} = (d_{90} - d_{10})/d_{50} = 1.2$. It is also worth noting that all mixtures had a volume fraction $\phi = 30 \text{ vol\%}$. From their work with bidisperse mixtures, the authors concluded that: ‘MR suspensions with special ratios of coarse and fine particles have higher shear stresses under a magnetic field than samples with monomodal powders.’ and that ‘The yield stress without field derived from oscillation experiments rises with the number of fine particles. However, at low field strengths (200 mT), the behavior is reversed and, at high field strengths (600 mT), no noticeable differences between the MR suspensions with different PSDs could be observed. The results demonstrate the complex mechanisms of the particle structure formation in MR suspensions.’.

Saldivar-Guerrero *et al* [27], working, experimentally, with IFFs (polystyrene particles dispersed in a ferrofluid), evaluated three classes of particles: a) monodisperse, with an average size of 11 μm , normalized polydispersity and $(d_{90} - d_{10})/d_{50} = 0.143$, b) monodisperse, with an average size of 3 μm and $(d_{90} - d_{10})/d_{50} = 0.186$ and c) polydisperse, with a size range between 0.56 and 4.5 μm and $(d_{90} - d_{10})/d_{50} = 0.873$. In this work, log-normal size distributions were used and the volumetric fractions $\phi = 17.5 \text{ vol\%}$, 25 vol%, and 30 vol% were investigated. In this context, the authors concluded that: ‘...the G' of the higher concentrated polydisperse fluid increased only marginally with the magnetic field.’ and that ‘...at high fields, the poisoning effect may be responsible for the weaker G' of the polydisperse suspensions compared to the monodisperse ones.’ The ‘poisoning effect’ mentioned by the authors comes from previous works: ‘The

effect that polydisperse particles might weaken the chains, as observed for higher values of the magnetic field, has recently been predicted in theoretical studies for a bidisperse model ferrofluid and was termed ‘poisoning effect’ (Kantorovich [28]). ‘It has been confirmed in molecular dynamics simulations for chain formation in standard ferrofluids’ (Wang and Holm [29]).

Tao [30], when investigating the physical mechanism to reduce the viscosity of dispersions, conducted experiments with iron nanoparticles with a diameter between 35 and 40 nm (typical of ferrofluid particles) dispersed in silicone oil, at a concentration of $\phi = 9$ vol%. The author concluded that: ‘The key (to reducing the viscosity of dispersions) is that the maximum volume fraction to be available for the suspended particles in the suspension increases with the particle size and the polydispersity in the PSD.’

Ekwebelam and See [31], in turn, experimentally studied the effects of PSDs on the magnetorheological response of IFFs prepared by mixtures of two spherical monodisperse particles: PMMA (fine, with an average size of 4.6 μm) and PE (coarse, with an average size of 80 μm). Such particles were dispersed in a ferrofluid (Ferrotec type EFH1), keeping the total volume fraction constant, at $\phi = 30$ vol%. Using oscillatory shear flow, the authors prepared five different mixtures: 1) 100:0 (fine particles only), 2) 75:25, 3) 50:50, 4) 25:75 and 5) 0:100 (coarse particles only). In this context, the authors conclude that: ‘...the G' and G'' moduli were dependent on the particle size as well as the proportion of small particles, with the highest storage modulus occurring for the monodisperse small particles.’ Although this paper covers a relatively high concentration, equivalent to most commercial MR fluids, it also did not involve single-modal distributions that differ only by the standard deviation values.

The work of Chiriac and Stoian [32] was, possibly, the first to experimentally focus on normal (Gaussian) size distributions with the same mean size and different variances, in magnetorheology. In practice, this means that these authors did not use bidisperse particles or any other mixtures that resulted in bimodal PSDs. Working with iron powders in the size range of 20–60 μm , the authors used sieves to fractionate these powders and then created distributions with controlled histograms. By preparing three different samples of MRF with a fixed volume fraction ($\phi = 10$ vol%) and maintaining the average size of 36 μm for the three formulations, but with different variances ($\sigma^2 = 0.2, 1.0$ or 5.0), the authors conclude that: ‘...Higher yield stresses were obtained in the case of MR fluids with the narrower PSDs compared to the MR fluids comprising particles with broader particles size distributions. In this respect, particles with narrower size distribution could lead to better performances of the MR fluid under a magnetic field. Nevertheless, the effect of particles size distribution on the MRF is still controversial, and the mechanism by which the particles size distribution influences the yield stress is not fully understood.’

Tang [4], in turn, experimentally studied MRF using micrometric iron particles of 2–3 μm and 45 μm in a volumetric concentration ϕ ranging between 35–43 vol%. From all the papers published until 2011, this was the first to present results of a

bimodal fluid with ϕ above 40 vol% (that is, a concentrated MRF). The particles followed a log-normal PSD, as shown in the figure 1 of this paper, but the width of the distributions was not reported. The author concludes that: ‘With the addition of small particles to a suitable concentration, the viscosity of the MRF decreases remarkably without the magnetic field.’ and that ‘In the same maximum packing, the yield stress can be dramatically augmented by using a bimodal MRF system.’

Juan de Vicente’s research group (Magnetic Soft Matter Group, F2N2Lab, Granada University) has systematically investigated the effects of polydispersity on magnetorheology. Their first work on this subject seems to be from Segovia-Gutierrez et al [33], where the authors compared the results of Brownian dynamics simulations with MRF experiments with a volumetric fraction $\phi = 5$ vol%. In this context, the authors utilized carbonyl iron powder (HQ, BASF SE) with a size of $0.9 \pm 0.3 \mu\text{m}$, describing it through a log-normal PSD. Among many conclusions, the authors pointed out that: ‘The monodisperse system crystallizes, while the polydispersity effectively suppresses it.’ However, in this study, there was no variation in the standard deviation of the particle sizes.

Sherman and Wereley [34] modified their code from previous simulations to investigate the effects of the standard deviation from log-normal size distributions on MRF performance. This was done by simulating a typical commercial volumetric fraction, $\phi = 30$ vol%, with carrier liquid viscosity of 0.1 Pa.s and keeping the median particle radius a_0 at 4 μm , over a wide range of standard deviation values ($\sigma = 0, 0.001, 0.0025, 0.005, 0.01, 0.025, 0.05, 0.1, 0.2$ and 0.3). In this paper, bimodal (or bidisperse) mixtures were not utilized, and the authors concluded that: ‘Based on these simulation results, we conclude that PSD has a substantial effect on the structure and performance of MRF, so that accuracy of simulation codes may improve when realistic PSDs are utilized.’ Although their work has brought valuable contributions, especially by simulating MR fluids similar to those used in commercial and industrial applications, their results did not show any obvious advantages or disadvantages, such as a considerable increase in the on-state yield stress.

Sarkar and Hirani [35] experimentally studied mixtures of two sizes of iron particles (MRF) at three concentrations: $\phi = 9$ vol%, 18 vol%, and 36 vol%. The particles used in the experiments were carbonyl iron powder and reduced iron powder (Aldrich #12310), Fe $\geq 99\%$ and, according to the authors: ‘The mean size and standard deviation of the “small-sized particle” distributions are 9.27 μm and 4.63 μm respectively. The mean size and standard deviation of the “large-sized particle” distributions are 120.85 μm and 56.05 μm respectively.’ Analyzing the morphology of the powders by SEM, the authors also add that: ‘The scanning electron microscope photographs.. shows that the “small-sized particles” are spherical in shape.. The “large-sized particles” are of flake shape. This flake type iron particle may create more friction...’ Therefore, it is possible to estimate a relative standard deviation $\alpha \approx 0.5$ for the carbonyl iron particles and $\alpha \approx 0.46$ to the flake-shaped particles. Finally, the authors concluded that: ‘At moderate shear rate MR fluid made of “large-sized particles” performs better only at low volume fractions of

iron particles compared to MR fluids made of low volume fraction “small-sized particles” and “mixed sized particles”. At moderate volume fraction “mixed sized particle” MR fluids provide the best performance among all three. With the increase in volume fraction of iron particles, the shear stress of MR fluids with “mixed sized particles” shows better performance compared to the MR fluids containing “small-sized particles” and “large-sized particles” at higher shear rate.’

Fernández-Toledano *et al* [36], continuing the work from Prof. Juan de Vicente’s research group (Granada University), used simulations to explore the effect of polydispersity in magnetorheology. Interestingly, instead of the well-known log-normal size distribution, which is commonly used to describe carbonyl iron powders, these authors chose to use the Schulz distribution (Schulz [37]), which was developed to describe molar mass distributions of polymers. Two volumetric concentrations were investigated: 10 vol% and 20 vol%, which were also associated with two conditions of polydispersity: $\sigma = 0$ (monodisperse) and $\sigma = 0.2$ (polydisperse). In this scenario, σ is the standard deviation of the distribution. It is also worth mentioning that the magnetic field strengths evaluated in this work were $H = 1 \text{ kA m}^{-1}$, 5.04 kA m^{-1} , and 10.2 kA m^{-1} , that is, weak to moderate fields. Throughout the work, the authors summed up very well the interest in this topic by asking: ‘...would ideally monodisperse MR fluids have better MR performance than their polydisperse counterparts for the same mean particle diameter?’ They also conclude: ‘From (shear) stress growth curves, static and dynamic yield stresses are determined, and rheograms are constructed... In polydisperse MR fluids, the number of connections is larger than in the monodisperse case, but, as an average, interparticle links are much weaker because of the topological limitations.’ Furthermore: ‘Overall, this work suggests that using monodisperse particles in the formulation of conventional MR fluids would not have any major effect in the yield stress nor the high shear behavior.’

Also, from Juan de Vicente’s research group, perhaps the most complete and detailed study on the effect of polydispersity so far is the work of Ruiz-López *et al* [38]. In their work, a wide range of standard deviations (σ) was evaluated, not only through simulations but also experimentally (from $\sigma = 0.38$ to $\sigma = 0.76$). Assuming a log-normal distribution for the MRF, the authors applied a strong magnetic field ($H = 885 \text{ kA m}^{-1}$), a value that is very close to the saturation of the carbonyl iron powders used in the preparation of the MRF. In this context, the reason for so many studies involving the effect of polydispersity on MRF is very well summarized by the authors: ‘...polydisperse MR fluids inherently exhibit a lower off-state viscosity than monodisperse MR fluids due to the different particle packing characteristics; larger packing fractions are achieved with polydisperse systems. This means that using polydisperse MR fluids, the particle volume fraction can be increased without increasing the off-state viscosity, hence developing a larger MR effect.’ Finally, in the polydispersity index (α) range studied by the authors, it is concluded that: ‘...the effect of the polydispersity on the yield stress can be considered as negligible in experiments..’ and also that ‘Analysis results on the particle cluster sizes and the particle radial distribution function show that increasing

the level of polydispersity of the MR system leads to a smaller average number of particles per cluster, but a higher packing density of the particles inside the clusters.’ However, one should note that the volumetric fraction studied by their simulations and rheological experiments was $\phi = 10 \text{ vol\%}$. This is a concentration that cannot be considered a diluted MRF but also does not approximate the concentrations which are used in commercial MR devices.

From the works indicated in Table 1, the results can be summarized as follows: some of the cited authors, such as Ruiz-López *et al* [38], worked experimentally with a very intense magnetic field, very close to the magnetic saturation, but with a concentration of magnetic material ranging from low to moderate (10 vol%). Thus, even though they explored an extensive range of the polydispersity index and molecular dynamics simulations corroborated their results, one should not extrapolate their conclusions for concentrations far above 10 vol%. Other authors, such as Fernández-Toledano *et al* [36], did not analyze MRF with magnetic fields greater than 10.2 kA m^{-1} (a relatively low intensity), despite having carried out simulations with MRF slightly more concentrated (up to 20 vol%). Furthermore, experimental results of rheometry were not presented in this work.

Other authors investigated mixtures of two or more particle sizes, especially the so-called bidisperse formulations. It has been known since the work of Farris [18] that using mixtures of bimodal, trimodal, or tetramodal particles can substantially reduce the relative viscosity of any concentrated suspension, increasing its concentration. However, this effect is only relevant for volume fractions greater than 35 vol% and particle size ratios of 1:5 (small:large), at least. This effect, commonly called the ‘Farris effect’, becomes increasingly large at concentrations above 50 vol% and, in the context of MRF, is advantageous to increasing the magnetorheological effect under an applied field. In this regard, Foister [39] pioneered (to the best of our knowledge) in patenting MRF based on bimodal mixtures.

However, the studies involving bidisperse mixtures did not focus on centering the PSDs around the same mode, varying only the standard deviation (width) of these distributions. In some experimental studies, such as the ones from Sarkar and Hirani [35], Tang [4], Ekwebellan and See [31], Trendler and Böse [26], and See *et al* [25], where MRF (or ERF) based on bidisperse mixtures were investigated, only Tang and Sarkar slightly exceeded a volumetric fraction $\phi > 35 \text{ vol\%}$. Mori *et al* [23], Wang *et al* [22], and Ota and Miyamoto [19], in turn, published simulation results with bidisperse ERF but without experimental results. In addition to not investigating the fluids experimentally, the authors did not surpass $\phi > 30 \text{ vol\%}$, and the size ratios between the particles did not exceed the proportion of 1:2.

Saldivar-Guerrero *et al* [27] and de Gans *et al* [24] experimentally investigated IFFs using magnetic fields of up to 245 kA m^{-1} , a value that is very close to what we used in our work. In the article by Saldivar-Guerrero *et al*, the authors studied a polydispersity range (measured through the $Span = 0.873$), and a volume fraction of PS microspheres dispersed in ferrofluid was characterized, up to 30 vol%.

Table 1. Works on the effects of polydispersity on ERF or MRF over the last years.

| Author/year references ^b | Fluid type | Phi (vol.%) | Distribution type, size range | Sigma range | Bidisperse? | Experimental / simulation / Exp + Sim? | Applied field intensity (H_0/E_0) | Does polydispersity strengthen the MR effect? |
|---|---|---------------|---|---------------------------|--|--|--|--|
| Manuel <i>et al</i> (This work), 2022 N.A. | MRF | 48.5 | Log-normal $\sim 7 \mu\text{m}$ | 0.44 0.67 1.06 | No | Experimental and Simulation ^a | $B \approx 0.57 \text{ T}$ | Yes |
| Ruiz-López <i>et al</i> 2016 [38] | MRF Carbonyl iron powder (CIP) in silicone oil | 10 | Log-normal 0.4–8 μm | 0.38–0.76 | No | Experimental and Simulation | 885 kA m ⁻¹ | '...a slight but non-significant increase of the yield stress is found for the highest polydispersities.' |
| Fernández-Toledano <i>et al</i> 2015 [36] | MRF | Up to 20 | Schulz 1.0 \pm 0.5 μm | 0.2 | No | Simulation | 1.0, 5.04, 10.2 kA m ⁻¹ | '...the effect of polydispersity is only relevant at the transition regime between magnetostatic to hydrodynamic control of the suspension structure.' |
| Sarkar & Hirani, 2015 [35] | MRF, CIP, and Iron reduced powder, Aldrich ^b 12310 | 9 18 36 | Log-normal 9.3 \pm 4.6 μm 121 \pm 56 μm | 0.5 (CIP) 0.46 (12310) | Yes (Small and Large particles exp. Study.) | Experimental | 0–152.4 kA m ⁻¹ | No |
| Sherman & Wereley, 2013 [34] | MRF | 30 | Log-normal $D_{50} = 4 \mu\text{m}$ | 0.0–0.3 | No | Simulation | * $M = 300 \text{ kA m}^{-1}$ (Magnetization) | '... PSD has a substantial effect on the structure and performance of MR fluids...' |
| Segovia-Gutiérrez <i>et al</i> 2013 [33] | MRF CIP | 5 | Log-normal (experiments) 0.9 \pm 0.3 μm | 0.05 | No | Experimental and Simulation | 0–350 kA m ⁻¹ | No (Based on figure 12 of these authors). |
| Tang, 2011 [4] | MRF | 35–43 | Log-normal 2–3; 45 μm | N.A. | Yes | Experimental | Unknown (N.A.) | Yes |
| Chiriac & Stoian, 2009 [32] | MRF spherical Fe particles (Mesh 325) | 10 | Normal (Gaussian) 36 \pm 24 μm | 0.45, 1.0, 2.24 | No | Experimental | 0–256 kA m ⁻¹ | No (Based on figure 4 of these authors). |

(Continued.)

Table 1. (Continued.)

| Author/year references ^b | Fluid type | Phi (vol.%) | Distribution type, size range | Sigma range | Bidisperse? | Experimental / simulation / Exp + Sim? | Applied field intensity (H_0/E_0) | Does polydispersity strengthen the MR effect? |
|-------------------------------------|---|--------------------|---|--|--------------------------|---|---|--|
| Ekwebelan and See, 2007 [31] | IFF: Ferrofluid, PPMA and PE | 30 | N.A. 4.6; 80 μm | N.A. | Yes | Experimental: Oscillatory shear flow | * $B = 0.54 \text{ T}$ | No |
| Tao 2007 [30] | MRF and ERF | 9 | N.A. 30–40 nm | N.A. | No | Experimental | $B = 0.15 \text{ T}$ or 0.38 T | 'The values of φ_{max} ... also increases with increasing polydispersity.' |
| Saldívar-Guerrero et al 2006 [27] | IFF PS microparticles in FF | 17.5, 25, 30 | Log-normal Monodisperse: 3 and 11 μm Polydisperse: 1.08 μm | $(d_{90}-d_{10})/d_{50}$ = 0.143, 0.186, 0.873 | Mono and Polydisperse | Experimental | 1–274 kA m^{-1} | No |
| Trendler & Böse 2005 [26] | MRF CIP | 30 | Log-normal $D_{50} = 1.8$ and $6.7 \mu\text{m}$ | $(d_{90}-d_{10})/d_{50} =$ 1.2 | Yes | Experimental | 0, 200, 600 mT | '...at high field strengths (600 mT), no noticeable differences between the MRS with different PSD could be observed.' |
| See et al 2002 [25] | ERF | 8 | N.A. 15 and 50 μm | N.A. | Yes | Experimental | $E = 0-2.5 \text{ kV mm}^{-1}$ (a.c. electric field, 50 Hz) | Yes |
| de Gans et al 2000 [24] | IFF FF: magnetite nanoparticles stabilized by oleic acid dispersed in decalin, IFF: Silica nanoparticles in FF. | 5.7 or 18 | N.A. 53 \pm 2 84 \pm 2 138 \pm 1 189 \pm 5 (nm) | N.A. | No | Experimental | 31, 77, 245 kA m^{-1} | No |

(Continued.)

Table 1. (Continued.)

| Author/year references ^b | Fluid type | Phi (vol.%) | Distribution type, size range | Sigma range | Bidisperse? | Experimental / simulation / Exp + Sim? | Applied field intensity (H_0/E_0) | Does polydispersity strengthen the MIR effect? |
|-------------------------------------|--|-------------|---|-----------------------|---------------------------------|--|--|--|
| Mori <i>et al</i> 1999 [23] | ERF | 11, 20, 30 | N.A. 1.9; 3.8 μm | N.A. | Yes 1:2 (Diameter ratio of 1:2) | Simulation | $E = 0.75, 1, 1.5, 2.0$ and 2.5 kV mm^{-1} | No |
| Wang <i>et al</i> 1997 [22] | ERF | 16, 24, 31 | Gaussian $0.5 \leq d_i/d_0 \leq 1.5$ ($d_i/d_0 = \text{certain diameter } d_i / \text{mean diameter } d_0$) | 0.0–3.0 | No | Simulation | Unknown (N.A.) | No |
| Lemaire <i>et al</i> 1995 [20] | MRF or IFF PS spheres with Fe_3O_4 inclusions in water Glass spheres in FF | 5 20 | N.A. (a) 0.5, 0.8, 1 μm (b) $45 \pm 5 \mu\text{m}$ (c) 5–50 μm | < 0.10 (monodisperse) | No | Experimental | 7.96, 9.15, 59.7 kA m^{-1} | No |
| Ota & Miyamoto, 1994 [19] | ERF Cubic particles | 20 | N.A. 1:1, 1:2, 2:3, 3:4, 4:5 | N.A. | Yes | Simulation | $E = 2 \text{ kV mm}^{-1}$ | No |

^a Our simulations involved computing the random close packing volume fraction (ϕ_{RCP}) through the standard deviation of each distribution and using it as an approximation of the maximum packing fraction (ϕ_{max}).

^b The authors claim values of variance, but silica prepared by the Stöber method is well known to produce monodisperse particles.

The results were obtained in oscillatory mode with amplitude sweeps, and the authors concluded that, in the case of polydisperse samples, a ‘poisoning effect’ occurs, which weakens and reduces the value of the elastic modulus. However, in the paper by de Gans *et al* [24], the use of nanometric Stöber silica dispersed in a ferrofluid cannot be considered a study of the effect of polydispersity, from our point of view, as the variance between the four size classes of the used silica is very small (as one can see in Table 1 from their paper).

Tao [30], in turn, described how an increase in polydispersity generates an increase in the maximum packing fraction and, consequently, a reduction in the relative viscosity of MRF or ERF. But, in his article, the magnetic field was applied to iron nanoparticles dispersed in pump oil, that is, a ferrofluid. As the concentration of particles was low (only 9 vol%), the effect of the magnetic field did not generate on-field yield stress but temporarily reduced the viscosity of the dispersion. In other words, a ‘negative’ MR effect was generated, which caused a reduction in viscosity.

Works such as those by Sherman and Wereley [34] (simulations), Segovia-Gutiérrez *et al* [33] (experimental and simulations), Chiriac and Stoian [32] (experimental), and Lemaire *et al* [20] (experimental) evaluated polydisperse MRF (and IFF) with standard deviation values up to 2.24 and under magnetic fields up to 350 kA m^{-1} (that is, moderate to high intensity). However, the concentration of iron particles did not exceed 30 vol%.

Therefore, it is clear how the results presented by the literature (summarized in Table 1) are conflicting, and, in this scenario, the need for further studies becomes evident. Aiming to offer another perspective, the present work is, to the best of our knowledge, the first to evaluate experimentally the effect of polydispersity in MRF with higher volumetric concentrations of carbonyl iron powder, maintaining the same mode and varying only the polydispersity. This work also appears to be the first study to demonstrate both an increase in yield stress under a magnetic field and a reduction in the viscosity in the absence of field by increasing the polydispersity.

3. Theoretical background

3.1. Polydispersity and PSDs

By analyzing particulate materials in detail, especially dense suspensions, one can easily see that they are seldom monodisperse, that is, their particles rarely have all the same size. Most of the time, these particles will have different sizes and shapes, being, therefore, polydisperse, as illustrated in figure 2. Such variations in size can be easily described by frequency distributions, the so-called PSDs [17, 40].

A PSD (shown in figure 3) is a probability density function (PDF) that expresses, in detail, the polydispersity of the analyzed material, that is, how different the particle sizes in that system are. Usually, log-normal distributions are used and along with important mathematical tools, such as mode, mean, median and standard deviation, these variations in particle sizes can be studied and quantified [41, 42].

A key piece in the optimization of MRF properties, PSDs are critical in several areas of science and engineering, often

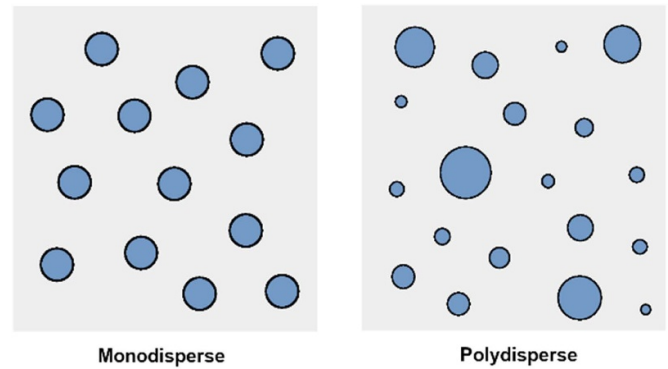


Figure 2. Monodisperse and polydisperse particles.

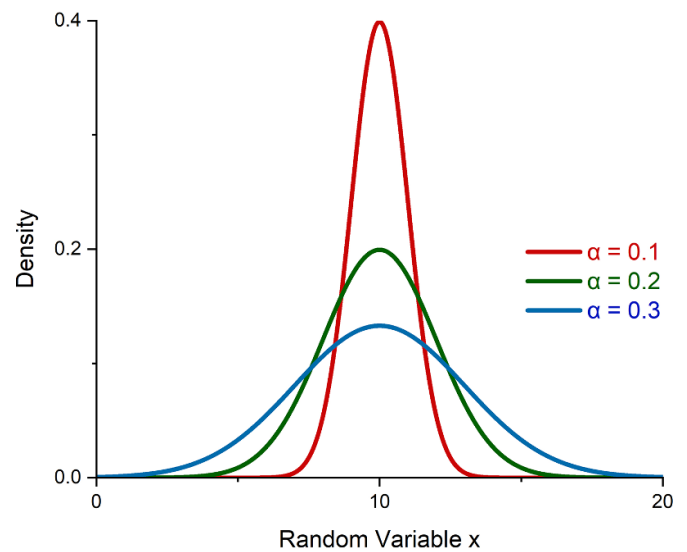


Figure 3. Particle size distributions (Gaussian): the greater the width of the distribution, the greater the value of the polydispersity index α .

appearing in soil and aerosol analysis, mining and even in the food industry [17]. Polymers and resins [43], paints [44] and drugs [45] are directly influenced by the size, quantity, and morphology of their particles.

When analyzing a PSD, several statistical parameters may be used. Among them, the polydispersity index α is the one that stands out the most: a direct measure of polydispersity, the higher the value of α , the greater the discrepancy in particle sizes. Its definition is presented below [17, 46]:

$$\alpha = \sqrt{\langle \Delta R^2 \rangle} / \langle R \rangle \quad (1)$$

where R is the particle radius, $\langle R^n \rangle = \int_{-\infty}^{\infty} R^n P(R) dR$ is the n -th moment of R , $\Delta R = R - \langle R \rangle$ and $\langle \Delta R^n \rangle = \int_{-\infty}^{\infty} \Delta R^n P(R) dR$.

It is worth noting that α takes many different forms in science and statistics, and this is due to many existing frequency distributions. However, its meaning is always the same: a measure of the spread of a variable around the mean [17].

As for the width of the distribution, one can use another important parameter, the span, to analyze it [47, 48]:

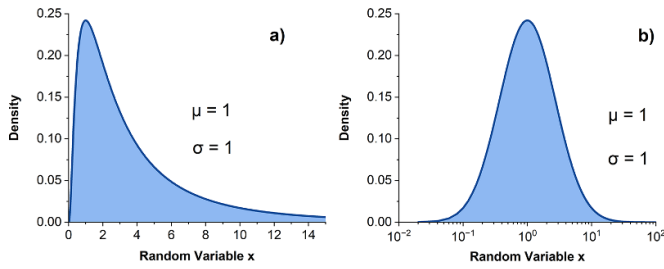


Figure 4. A log-normal distribution in: (a) linear scale and (b) logarithmic scale.

$$Span = \frac{D_{90} - D_{10}}{D_{50}} \quad (2)$$

where D_{90} is the particle size corresponding to the 90th percentile, D_{10} is the size of the 10th percentile and D_{50} , the median size. The span is directly related to variations in particle sizes and works similarly to α : the higher its value, the greater the polydispersity of the studied material.

The shape of a PSD, in turn, is generally determined by the skewness S and by the kurtosis K , respectively. Their definitions are given below [46, 49]:

$$S = \frac{\langle \Delta R^3 \rangle}{\langle \Delta R^2 \rangle^{3/2}} \quad (3)$$

$$K = \frac{\langle \Delta R^4 \rangle}{\langle \Delta R^2 \rangle^2}. \quad (4)$$

In general, the skewness measures the distortion of a frequency distribution, that is, how much it deviates from symmetry: positive values indicate a larger fraction of small particles, negative skewness indicates a larger fraction of large particles, and $S = 0$ indicates a symmetric distribution [49, 50].

Kurtosis, in turn, is commonly interpreted as a measure of peakedness: a positive value generates distributions with higher peaks and larger tails, while negative values generate more flattened curves, with smaller tails [50, 51].

3.2. Log-normal distributions

Although several PDFs can be used to describe variations in particle sizes, most of the encountered data in the literature are skewed, which is common when the mean values are low, strictly positive, and with wide variances. In this context, to properly represent a PSD, the use of log-normal distributions (illustrated in figure 4) is common practice [40, 42].

As one can see, unlike the symmetrical normal distributions, log-normal distributions are asymmetric with $S > 0$. The distribution's main properties are summarized in table 2: [42, 46, 52–54].

Thus, one can see how log-normal distributions are a viable model for studying the polydispersity of particulate materials. However, when preparing MRF based on carbonyl iron powders, it is necessary to differentiate which mixtures are bimodal (with two main particle sizes) and which are unimodal (with only one predominant particle size). The definitions

Table 2. Properties of a log-normal distribution.

| Parameters | Random Variable x , Mean (μ) of $\ln(x)$ and Standard Deviation (σ) of $\ln(x)$ |
|---|---|
| Range | $0 < x < \infty; \sigma > 0$ |
| PDF | $f(x) = \begin{cases} \frac{1}{x\sigma\sqrt{2\pi}} \exp\left(-\frac{1}{2\sigma^2}(\ln(x) - \mu)^2\right), & x > 0 \\ 0, & x \leq 0 \end{cases}$ |
| Mean | $E(x) = e^{\left(\mu + \frac{1}{2}\sigma^2\right)}$ |
| Mode | $\text{Mode}(x) = e^{\left(\mu - \sigma^2\right)}$ |
| Median | $\text{Med}(x) = e^\mu$ |
| Variance | $\text{Var}(x) = e^{\left(2\mu + \sigma^2\right)} \cdot \left(e^{\sigma^2} - 1\right)$ |
| Coefficient of Variation (Polydispersity Index) | $\alpha = \sqrt{e^{\sigma^2} - 1}$ |
| Skewness | $S = \left(e^{\sigma^2} + 2\right) \sqrt{e^{\sigma^2} - 1}$ |
| Kurtosis | $K = e^{4\sigma^2} + 2e^{3\sigma^2} + 3e^{2\sigma^2} - 3$ |

presented throughout this section hold only for unimodal distributions.

It is important to emphasize that bimodal blends are a traditional and well-established way of increasing the concentration of dispersed solids. By using different size classes, it is possible to maintain or even reduce the relative viscosity for the same volume fraction under certain conditions. As examples of works involving bimodal mixtures, we can cite Trendler and Böse [26] (see figure 1 of their paper) and the US Patent by Foister [39] (figures 7 and 8 of his patent).

As for unimodal blends, the patent by Kintz and Forehand [55] demonstrates the effect of increasing the polydispersity of a size distribution and the advantages of such an approach (see figures 2–9 of their patent). However, the *Span* presented in this patent does not exceed 2.683, a relatively low value.

Combined with the conflicting results presented in the literature and aiming to offer a new perspective on PSD influence on MRF's properties, this work prepares three concentrated fluids ($\phi > 45$ vol%) with different degrees of polydispersity but centered around the same mode. Three blends of carbonyl iron powder (described by log-normal distributions) will be dispersed in polyalphaolefin oil, totaling 48.5 vol%. Its rheology will then be analyzed and quantified in the presence and absence of an external magnetic field.

4. Experimental

4.1. Materials

To prepare the MRF, carbonyl iron powder (BASF SE) was used as a solid phase, in three different grades: 1, 2, and 3. To obtain an effectively polydisperse fluid, different blends were prepared by mixing the adequate amounts of each powder, totaling 150 g. The size distributions were obtained through low-angle laser light scattering (LALLS: Malvern Mastersizer Micro). The carrier liquid was a polyalphaolefin oil (Durasyn PAO 162, INEOS) used together with thixotropic additives (organomodified clays) and polymeric dispersants. The

Table 3. —The amounts of each powder used to prepare the blends.

| Blends | Powder 1 (g) | Powder 2 (g) | Powder 3 (g) | Total (g) |
|--------|--------------|--------------|--------------|-----------|
| A | 0 | 150 | 0 | 150 |
| B | 25 | 100 | 25 | 150 |
| C | 50 | 50 | 50 | 150 |

amounts of powder used to prepare each blend are shown in table 3:

4.2. Preparation of the MRF

The MRFs were prepared based on previous work from Ierardi and Bombard [56] by dispersing the appropriate amounts of each powder, shown in table 3, in PAO-2, totaling 48.5 vol%. Mixtures A, B, and C were then homogenized with an IKA Ultra Turrax T-18 mechanical disperser, followed by the addition of the thixotropic additives and further homogenization. The amounts of carrier liquid and additives (dispersant and thixotropic) were maintained during each preparation, following a recipe that is similar to formulation #12 in the US Patent ‘Magnetorheological Liquid’, by Oetter *et al* [57]. The reason for maintaining the amounts of all other components during the MRF formulation was precisely to isolate the effect of polydispersity on the viscosity response in the absence of a magnetic field. If the content of additives were different in each formulation, it would be difficult to attribute any results to the polydispersity.

4.3. Rheometry

After preparing the MRF, each sample was submitted to tests in the Anton Paar—Physica MCR 301 rheometer, from the Rheology Laboratory of the Federal University of Itajubá, at a temperature $T = 25\text{ }^{\circ}\text{C}$. Shear stress ramps under applied magnetic field, and shear rate ramps without field were performed, to analyze the effects of polydispersity on the on-state yield stress and on the off-state plastic viscosity, respectively. The magnetic flux density was estimated to be $B \approx 0.57\text{ Tesla}$, considering the relative permeability $\mu_{\text{rel}} = 7.8$. See the supplementary material for more details. (In air, without any MRF sample between the plates, we measured $B_{\text{air}} = 0.34\text{ T}$, thus $H_{\text{air}} = 3,400\text{ Oe} \approx 270\text{ kA m}^{-1}$ *)

Yield stress measurements were performed at three intervals: firstly, the rheometer was operated for 1 min, at a shear rate of 5 s^{-1} , to erase the rheological history of the sample. Then, the plate was stopped (without rotation, zero shear rate) for 30 s, and the electric current was increased, at a logarithmic rate, from 20 mA to 2 A. Finally, a linear shear stress ramp was performed for 400 s (100 Pa s^{-1} , 1 s per point), from 20 kPa to 60 kPa.

* The magnetorheological cell used to carry out the measurements was one of the first commercial versions of the rheometer manufacturer, and it is not possible to measure the B field in the ideal way, with the Hall effect probe and the MRF sample simultaneously. The only possible estimate of the value of the magnetic field was measured with the gap empty, in air, without MRF between the cell plates.

The off-state viscosity curves, in turn, were obtained through a linear ramp (100 points, measured at 6 s intervals), with the shear rate ranging from $0\text{--}1000\text{ s}^{-1}$. All the data were treated with the Rheoplus® (Anton Paar) and Origin® (Microcal) software.

4.4. Sedimentation and stability

Two experiments were performed to evaluate the stability against sedimentation: first, about 15 ml of each MRF sample was placed in test tubes to sediment at rest, under normal gravity. Then, observing the tubes daily and visually throughout a month, the height of the sediment was measured. The sedimentation was considered complete when there was no further change in the height of the sediment after three successive readings. This is one of the usual ways of evaluating the stability of an MRF when it comes to sedimentation [58–62].

In addition, an instrumental analysis was performed with the aid of the Turbiscan Lab equipment (Formulation, Toulouse, France). Each sample was subjected to back-scattered infrared light ($\lambda = 850\text{ nm}$) for two weeks, and their destabilization kinetics were analyzed. During the first 24 h, each reading was taken every 10 min, and after that, one reading was taken once a week. After the samples finished sedimenting, their turbiscan stability indexes (TSI) were calculated.

4.5. Simulations

Following the rheological characterization, the random close packing volume fractions were calculated with the help of two algorithms: (a) SpherePack1D (available at <https://sourceforge.net/projects/spherepack1d/>), which is based on the work of Farr and Groot [63] and Farr [64] and (b) a random close packing algorithm based on the computational methods of Xu, Blawdziewicz, and O’Hern [65], and Desmond and Weeks [46, 66].

5. Results and discussion: experimental

5.1. Polydispersity of the carbonyl iron powders

From the data obtained by LALLS, it was possible to construct log-normal PSDs and cumulative distributions (CDF) for each powder, illustrated in figures 5 and 6. In this context, CDF are useful because, sometimes, the data at the tails of a PSD can show some statistical noise. By using these cumulative curves, one can avoid losing any information [67].

An initial analysis of figure 5 reveals that the sizes range from 500 nm to 300 μm and that the PSD are predominantly unimodal and polydisperse, except for powder 1, whose distribution is bimodal. The prevailing sizes, corresponding to the geometric modes of these distributions, are 6.89 μm for powder 2 and 20.68 μm for powder 3. Powder 1, in turn, has two modes: 2.0 μm and 11.93 μm .

One can also note that powder 3 has greater polydispersity since the width of its distribution is the largest among the three.

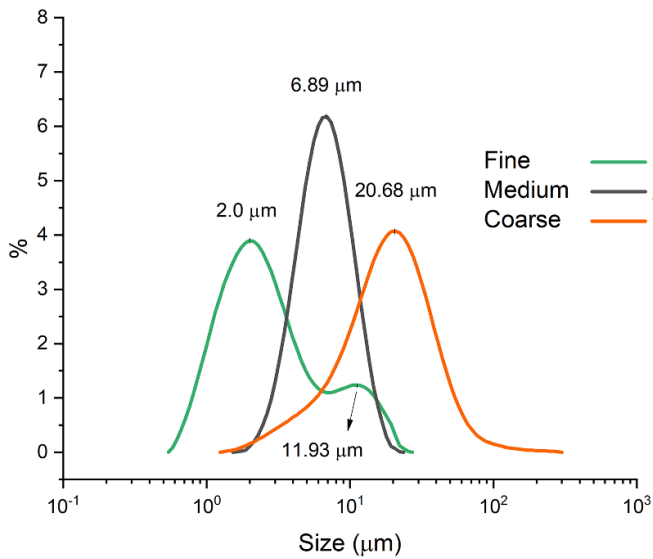


Figure 5. Particle size distributions of each carbonyl iron powder.

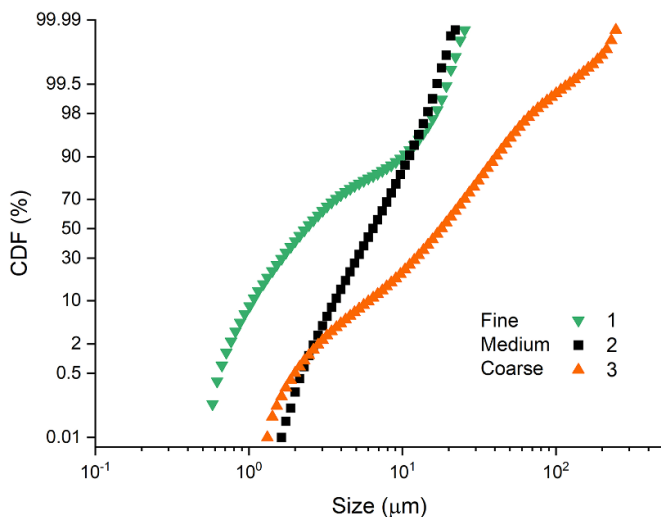


Figure 6. Cumulative frequency curves of each carbonyl iron powder.

Powder 2, in turn, has less polydispersity, because of the smaller width. This trend can be confirmed by analyzing the CDF in figure 6: in these curves, the median is easily identified by drawing a horizontal line at 50%. Promptly, it can also be seen that the geometric modes are the same as in the PDFs and that the size ranges are maintained.

Polydispersity, in turn, can be analyzed through the slope: on a logarithmic scale, the lower the slope of a CDF, the greater the polydispersity of that system [68]. In magnetorheology, this was confirmed by the work of Kintz and Forehand [69], where the span and R^2 of 9 cumulative curves were analyzed and quantified. As expected, greater polydispersity values were associated with lower slope values. Therefore, curve 3 shows greater polydispersity, and curve 1, the smallest, reiterating the trend observed in figure 5. It is also worth mentioning that curves 1 and 3 are not perfectly straight and this is due to distortions present in their PSD: curve 1 is bimodal and curve 3 is slightly skewed to the right.

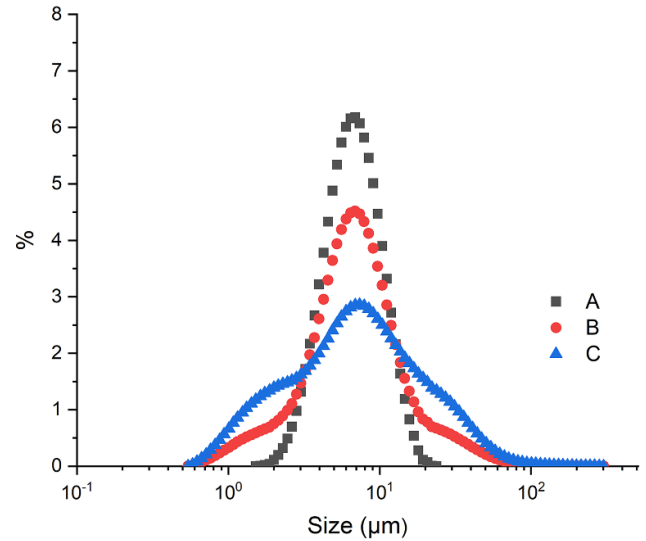


Figure 7. Particle size distributions of each blend.

5.2. Polydispersity of the blends

After mixing the powders, according to the amounts indicated in table 3, the distributions became even more polydisperse. The log-normal PSD of each blend is illustrated in figure 7:

One can immediately notice that the distributions have the same geometric mode since all the peaks are centered on the same value, at $\sim 7 \mu\text{m}$. With that in mind, it can be inferred that the only differences between the MRF are their PSDs. It can also be said that blend C has the highest polydispersity, due to its greater width, while blend A has the smallest.

The CDF shown in figure 8(a) reiterates these observations: at $7 \mu\text{m}$, all curves intersect, indicating that the geometric mode is common to all three distributions. Furthermore, in the region between 10% and 90%, one can notice that the slope of curve C is the smallest, that is, it is more polydisperse than the others, while curve A, with the greatest slope, is the least polydisperse. The span of each curve, expressed in figure 8(a), corroborates this.

Through the Origin® software, it is possible to compute the log-normal cumulative curves with the help of equation (5). These curves are used to determine the value of the standard deviation σ of each blend and to calculate their polydispersity indexes ($\alpha = \sqrt{e^{\sigma^2} - 1}$):

$$CDF = y_0 + A \int_0^x \frac{1}{x\sigma\sqrt{2\pi}} \exp\left(-\frac{1}{2\sigma^2}(\ln(x) - \mu)^2\right) dx \quad (5)$$

where y_0 is the offset parameter and A is the amplitude.

Such cumulative curves are shown in figure 8(b), and the values of α are shown in table 4. Again, one can see that blend A is the least polydisperse, and that blend C is the most polydisperse, which corroborates the previous statements.

5.3. Magnetorheology

Through the rheometer, it was possible to quantitatively analyze the effect of broadening the blend's distributions

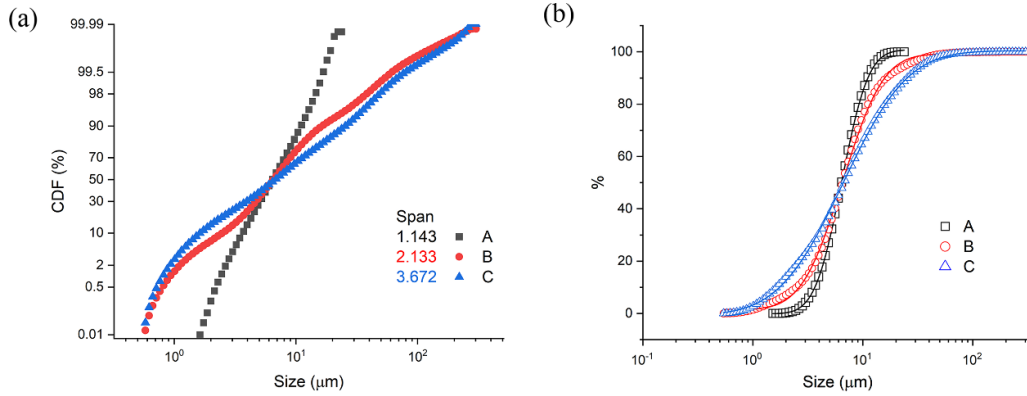


Figure 8. (a) Cumulative frequency curves of each blend. (b) Log-normal cumulative curves of each blend.

Table 4. Statistical parameters and rheological properties of each MRF.

| Blend | R ² | σ (Std. Dev.) | Span | α | Off-state plastic viscosity (Pa.s) | Yield stress @ B \approx 0.57 T (kPa) |
|-------|----------------|----------------------|-------|----------|------------------------------------|---|
| A | 0.99995 | 0.440 \pm 0.002 | 1.143 | 0.46 | 4.8 | 30.0 \pm 0.5 |
| B | 0.99918 | 0.670 \pm 0.009 | 2.133 | 0.75 | 1.2 | 35 \pm 1 |
| C | 0.99972 | 1.061 \pm 0.008 | 3.672 | 1.44 | 0.5 | 42 \pm 2 |

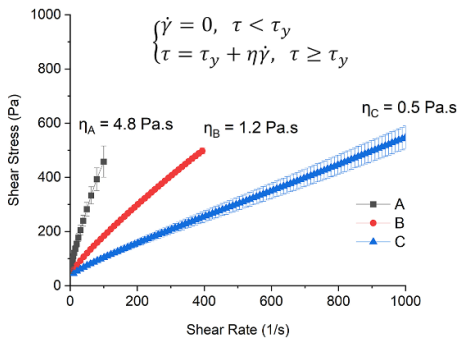


Figure 9. Off-state flow curves of each MRF.

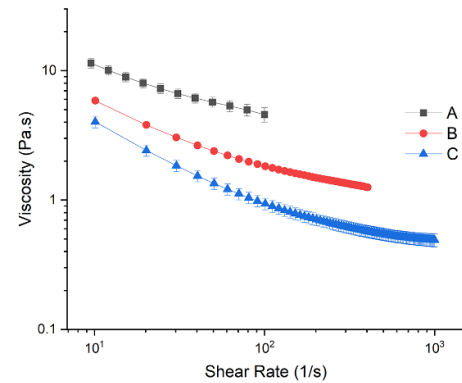


Figure 10. Viscosity curves (off-state) of each MRF.

by constructing flow curves and viscosity curves (off-state), which are illustrated in figures 9 and 10.

Figure 9 depicts the off-state flow curves of the three MRF, allowing one to obtain the off-state plastic viscosities for each one.

At sufficiently high shear rates, the behavior of each MRF can be described, in a very simplified way, by the Bingham model [6, 70].

$$\begin{cases} \dot{\gamma} = 0, \tau < \tau_y \\ \tau = \tau_y + \eta_p \dot{\gamma}, \tau \geq \tau_y \end{cases} \quad (6)$$

where τ is the shear stress, τ_y is the yield stress, η_p is the plastic viscosity and $\dot{\gamma}$ is the shear rate.

Through equation (6), one can see that this model shows a linear behavior since τ_y and η_p are constants and it can be concluded, therefore, that the slope of each curve corresponds to the apparent viscosities of the fluids. Usually, it is recommended to plot the flow curves in a log \times log scale but, in this

case, a linear \times linear scale better demonstrates the differences in the slope values. One can, of course, question whether Bingham's model is valid, but the reduction of the plastic viscosity with an increase in polydispersity is evident.

It can also be noted that lower relative viscosities are associated with wider size distributions, due to an increase in polydispersity and to different packing characteristics of their particles [16]. This behavior is well documented in the literature and can be explained, among several existing models, by the Krieger–Dougherty equation [71]:

$$\eta_{rel} = \left(1 - \frac{\phi}{\phi_{max}}\right)^{-[\eta] \cdot \phi_{max}} \quad (7)$$

where η_{rel} is the relative viscosity, $[\eta]$ is the intrinsic viscosity, ϕ is the volume fraction and ϕ_{max} is the maximum packing fraction.

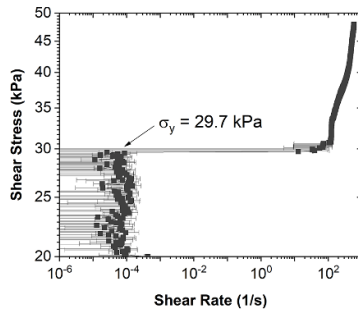


Figure 11. On-state yield stress curve of fluid A.

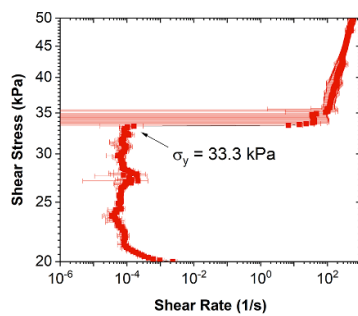


Figure 12. On-state yield stress curve of fluid B.

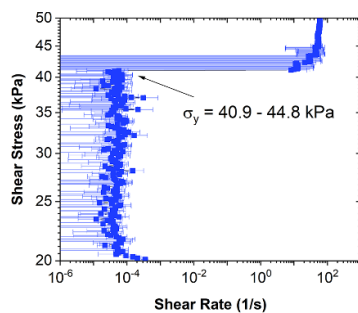


Figure 13. On-state yield stress curve of fluid C.

By analyzing the curves in figure 10, one can also observe a significant drop in viscosity through an increase in the shear rate. This non-Newtonian behavior, the so-called shear-thinning, is typical of colloidal suspensions and is expected for MRF in the absence of an applied magnetic field [2, 6, 72].

It is also possible to notice a significant drop in viscosity with the widening of the PSD: fluid A, which has a narrower distribution, has the greater viscosity, while fluid C has the lowest.

Finally, the on-state yield stresses of each MRF can be obtained from figures 11–13.

In a yield stress curve, the sudden change of several orders of magnitude in the shear rate value, from about 10^{-4} s^{-1} to above $\sim 5 \text{ s}^{-1}$ signals the point at which the applied stress was sufficiently large ($\tau > \tau_y$) to break the structuring of the material, causing it to flow ($\dot{\gamma} > 0.0005$). This value corresponds to the yield stress itself and represents, in a MRF under field, the point at which the chain-like structures break [2, 11, 16]. It is also worth mentioning that the measurements were made in triplicate.

As the rheometer operates in controlled shear stress mode (CSS) and the shear stress is below the yield stress value, there is a lot of noise in the shear rate. However, when the shear stress becomes greater than the yield stress, the noise tends to decrease. The (on) yield stress and the (off) plastic viscosity values are summarized in table 4, along with all the statistical parameters of the log-normal distributions. Promptly, one can see that the yield stress grows significantly with an increase in polydispersity: fluid C, which has the widest PSD, has the highest yield stress, while fluid A, with the narrowest distribution, has the smallest.

6. Results and discussion: simulations

During the study of particulate materials, the maximum packing fraction ϕ_{\max} is one of the most relevant parameters to explain the reduction in viscosity, as expressed in equation (7). However, it is not a well-defined parameter, and its value depends both on the spatial distribution of the elements and on the flow history [73]. In this paper, since the particles are spherical and well lubricated, the value of ϕ_{\max} can be approximated by the random close packing volume fraction [17] ϕ_{RCP} and, therefore, all the simulations will deal with the value of ϕ_{RCP} .

6.1. Rod distribution algorithm (1D)

Using the program SpherePack1D (available at <https://sourceforge.net/projects/spherepack1d/>), it was possible to calculate the maximum random close packing fraction (ϕ_{RCP}) of each MRF through a distribution of diameters (rod distribution), which is described in Farr [63]. By employing the values of the standard deviations in table 4, it was found that the ϕ_{RCP} of each fluid is: 69.6% (fluid A), 74.0% (fluid B), and 81.2% (fluid C).

6.2. Random close packing algorithm (3D)

We conjecture that our off-state viscosity results may be explainable by considering the random close packing value for each PSD. That is, all of our samples are at a fixed volume fraction of 48.5%, and this can be compared to the random close packing volume fraction which should depend on the PSDs.

To determine the random close packing volume fraction for our three PSDs, we follow the computational methods of Xu *et al* [65], and Desmond and Weeks [46, 66]. Briefly, we start by taking the experimentally determined PSD (in other words, the data shown in figures 7 and 8(a)) and generating N random particle radii consistent with the desired PSD. We randomly place these N particles in a large cubical box with periodic boundary conditions, with the box size chosen so that the starting volume fraction is 1% (or 0.1% if the ratio of largest particle radius to smallest is larger than 50).

Starting from this initial condition, we gradually increase the size of all particles in small steps and move particles that overlap until we reach a close packed state. Specifically, at each size increase step, we expand the particles by multiplying their radii by $1 + \epsilon$, so that the PSD remains unchanged

except for the overall scale. In particular, the polydispersity, skewness, and kurtosis remain unchanged. After an expansion step, we then examine all particles that are touching another particle. We treat each particle as a soft particle with an interaction potential that is equal to the square of the overlap of each particle pair. That is, this potential goes smoothly to zero at the separation distance r_{ij} equal to the sum of the two particle radii ($R_i + R_j$); and the potential increases as $(R_i + R_j - r_{ij})^2$ when particles overlap. We consider overlapping particles in random order, moving an individual particle via two conjugate gradient steps to minimize the interaction energy, hopefully to zero. For any particles not in contact with any other particles, we move them a small random step (if that does not cause any new overlaps). This random step facilitates finding dense packings. When the total system energy is reduced below a numerical tolerance, the next expansion step is tried.

At some point, the total system energy cannot be reduced below the chosen tolerance. The program then reverts to a lower volume fraction, reduces the expansion factor ϵ , and then tries another expansion step. This is repeated until no expansion seems to be possible. At this point, the computation slightly decreases the size of all particles (by a uniform multiplicative factor) so that the energy is strictly zero, which is to say that no particles are overlapping at all, and this determines the final random close packing state for the N particles.

We then repeat this process many times for $N = 300, 400, 800,$ and 1600 ; each repetition is with a new set of N random particle sizes drawn from the desired PSD. For each N , we then compute the mean observed random close packing volume fraction. Following the work of Desmond and Weeks [66], we note that the mean volume fraction grows linearly with $N^{-1/3}$, thus allowing us to extrapolate to the $N \rightarrow \infty$ limit.

For a perfectly monodisperse packing, this algorithm yields $\phi_{RCP} = 63.6 \pm 0.1\%$, in good agreement with prior observations. For our experimentally measured PSDs, we find $\phi_{RCP} = 67.3 \pm 0.2\%$ (fluid A), $\phi_{RCP} = 71.4 \pm 5.7\%$ (fluid B), and $\phi_{RCP} = 79.6 \pm 5.0\%$ (fluid C). The significantly larger uncertainties for fluids B and C are due to the difficulty in adequately sampling such broad PSDs. That being said, clearly the more polydisperse size distributions can be packed to larger values for their random close packing volume fraction. This is quite consistent with our observation that these samples have lower off-state viscosities: essentially, they have more free volume to rearrange and flow, as (at constant volume fraction 48.5%) they are farther from their maximum possible volume fractions.

Table 5 compares the random close packing volume fractions calculated by each algorithm. It is worth noting, however, that there is a discrepancy between the methods. For Farr and Groot [63], the random close packing was computed using a log-normal distribution and the standard deviations obtained from equation 5. The method from Desmond and Weeks [46], in turn, uses the actual histograms (which are not perfectly log-normal) to compute the random close packing.

It is worth mentioning that, although the values calculated by the algorithms are slightly different, the trend presented by both is the same: an increase in the maximum random close

Table 5. A comparison between the values calculated by the rod distribution algorithm (1D, Farr and Groot [63]) and the random close packing algorithm (3D, Desmond and Weeks [46]).

| MRF | ϕ_{RCP} (1D) | ϕ_{RCP} (3D) |
|-----|-------------------|-------------------|
| A | 69.6% | $67.3 \pm 0.2\%$ |
| B | 74.0% | $71.4 \pm 5.7\%$ |
| C | 81.2% | $79.6 \pm 5.0\%$ |

packing fraction with an increasing polydispersity of each size blend. Through these results, it is possible to explain the reduction in the viscosity of each MRF.

7. The effect of polydispersity on the suspension's stability

7.1. Sedimentation ratio

Stability is a term that can be confusing when it comes to magnetorheology. Unlike ferrofluids, colloidal dispersions of nanometric particles that, when adequately prepared, are stable in terms of particle coagulation, MRF are classified as non-Brownian dispersions since the most common materials used during preparation are carbonyl iron powders, with typical sizes between 1–20 μm . Therefore, they tend not to be stable against settling.

However, we do not refer to colloidal stability, that is, the aggregation of individual particles in flocs, but rather the stability of two phases with very different densities: a dense phase of micrometric iron ($\rho \approx 7860 \text{ kg/m}^3$) and a phase of synthetic, low polarity liquid (polyalphaolefin oil with a density of 796 kg m^{-3}). In very low concentrations (about 1 vol%), one could use the classical Stokes' equation to describe the velocity of sedimentation v_{sed} of spheres in Newtonian fluids:

$$v_{\text{sed}} = \frac{g(\rho_s - \rho_l)d^2}{18\eta} \quad (8)$$

where g is the acceleration of gravity, ρ the densities of the solid phase (s) and liquid phase (l), respectively; d is the particle's diameter and η is the viscosity of the surrounding fluid.

However, we have a very high concentration of solid particles ($\phi = 0.485$), and the most significant limitation of Stokes' equation, in this case, is the so-called 'hindered settling' since the particles start to collide. In addition, there's also polydispersity, which affects packing efficiency. Although there are theoretical models that attempt to correct the Stokes equation with hindered settling, few models include the effect of polydispersity.

In this context, the stabilities of each suspension can be analyzed visually: according to the procedures described in section 4.4, immediately after preparing the samples, the MRF were transferred to transparent, cylindrical test tubes (inner diameter of 14 mm and height of 104 mm) and the boundary between the sediment and the oil phase was recorded over time, every 24 h. The sedimentation ratio (S.R.) was then computed as:

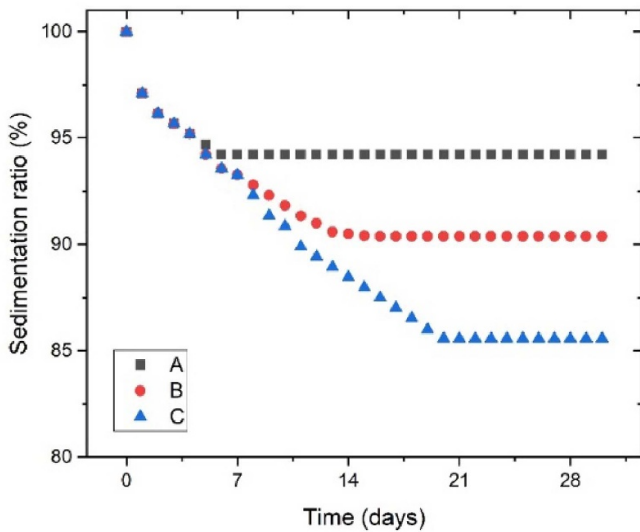


Figure 14. The sedimentation ratio as a function of time for the three MRF, visually measured through the sediment height method. The test tubes were under rest, at normal gravity and room temperature ($20 \pm 5^\circ\text{C}$).

$$S.R. = \left[\frac{\text{sediment mudline height (mm)}}{\text{initial height MRF (mm)}} \right] \times 100. \quad (9)$$

Figure 14 illustrates the sedimentation of the three blends according to the procedure described in section 4.

From figure 14, one can see that: (1) while blend A took less than a week (6 d) to reach the end of its sedimentation, blends B and C took about two and three weeks, respectively. The sedimentation of blend B took up to 15 d, while that of blend C took 20 d. (2) The sedimentation ratio decreases by increasing polydispersity; the greater the polydispersity, the greater the height of the oil layer (supernatant). This was already expected since broader PSDs show greater maximum packing fractions, as their particles are more compacted, reducing the height of sediment. (3) The final sediment ratios were 94.2%, 90.4%, and 85.6% for blends A, B, and C, respectively.

Thus, the experiment confirms, at least qualitatively, the order of magnitude of ϕ_{max} (RCP) predicted by the simulations from Farr and Groot [63] and Desmond and Weeks [46]: the greater the maximum packing fraction, the more compact the sediment and, thus, the smaller its volume.

It is also worth noting that the sedimentation curves can be divided into five distinct regions: 1) the first 24 h, where it is impossible to notice differences between the three mixtures, and the particles begin to sediment individually, forming a network of flocs. 2) the interval between the second and fourth days, where the sediment/liquid interface (mudline) moves at an almost constant rate, with the flocs settling at the same speed. In this interval, the three mixtures show nearly identical settling behavior, and the slope of this region can be treated as the sedimentation rate. For blend A, this rate was 0.48%/day, and for blends B and C, 0.54%/day and 0.7%/day, respectively. 3) the fifth day, where A already differentiates itself from the others and stops its sedimentation. 4) the interval between the fifth and the seventh day, where mixtures B

Table 6. Stability grades according to the turbiscan index.

| TSI value | 0–0.5 | 0.5–1.0 | 1.0–3.0 | 3.0–10.0 | >10.0 |
|-----------------|-------|---------|---------|----------|-------|
| Stability grade | A+ | A | B | C | D |

and C remain at the same level of sedimentation and start to differentiate, continuing to settle until almost three weeks. 5) the 6th, 15th, and 20th day for blends A, B, and C, respectively, where the sedimentation ends, and any changes are no longer visible [74].

The volume of sediment in the final region is called terminal sediment volume (TSV). It can be interpreted as the fraction of the initial volume that is present in the sediment [74–76]. The following expression can be used to compute the TSV:

$$TSV = \phi \frac{H_0}{H_{(t \rightarrow \infty)}} = \frac{\phi}{S.R._{\text{Final}}} \quad (10)$$

where ϕ is the volume fraction of solids (48.5 vol% for all mixtures), H_0 is the height of the column when settling began, $H_{(t \rightarrow \infty)}$ is the height after settling is complete, and $S.R._{\text{Final}}$ is the sedimentation ratio after the height of the sediment is stable. The TSV values were, therefore, 0.515 for blend A, 0.536 for blend B, and 0.567 for blend C. As expected, with the higher polydispersity, the more compact the sediment and higher the value of TSV.

7.2. Destabilization kinetics – TSI (global)

Another valuable way to analyze sedimentation is by using the Turbiscan equipment (Formulation France) and their so-called TSI [77]. This index measures the colloidal stability of dispersions and emulsions through transmitted or backscattered infrared light ($\lambda = 850\text{nm}$) [78]. Many authors have already used this type of analysis to assess the stability of MR fluids against sedimentation, such as Kim and Choi [79], Dong et al [80], Cvek et al [81].

The destabilization kinetics of the three samples can be easily compared through the TSI. According to the instrument's operation manual [82]: 'These kinetics are based on the following computation, comparing every scan of a measurement to the previous one, on the selected height, and dividing the result by the total selected height in order to obtain a result which does not depend on the quantity of product in the measuring cell.' Mathematically, the TSI can be expressed as:

$$TSI = \frac{\sum_h |scan_i(h) - scan_{i-1}(h)|}{H} \quad (11)$$

where H is the total height of the sample in the test tube, and $scan_i$ is the result of each measurement (vertical optical transmitted or backscattered light) from the Turbiscan. The user defines the intervals, which can be adjusted through the instrument's software.

Also, according to the manufacturer, one can classify the stability of dispersions through the TSI values, as shown in table 6 [82]:

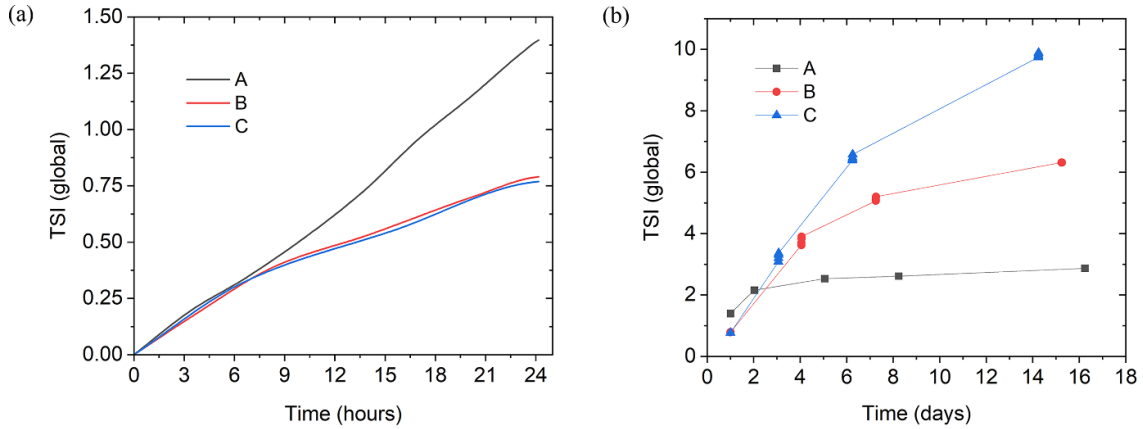


Figure 15. (a) The TSI (global) as a function of time, measured during the first 24 h. Readings were taken each 10 min. (b) The TSI (global) as a function of time, measured after the first 24 h.

From figure 15(a), we can see that, at the beginning of the test, there is no difference in stability for the three MRF samples, and all of them would be graded A+ (TSI < 0.5). But, after six hours, these samples start to differentiate: samples B and C are graded A ($0.5 < \text{TSI} < 1.0$), and sample A, after 18 h, is graded B (TSI > 1.0).

However, from figure 15(b), one can see that the destabilization kinetics differs significantly after the first day: fluid A, after two weeks of sedimentation, is graded B (TSI < 3.0), while samples B and C are graded C ($3.0 < \text{TSI} < 10.0$). After 15 d, sample C would likely change to grade D (TSI > 10.0).

Although the stability test with turbiscan is very sensitive and detects changes at the top of the test tubes and in the middle and bottom, the TSI values confirm the same trend observed during the sedimentation tests: sample A stops sedimenting more quickly than the other samples. Furthermore, the changes in its TSI values are negligible after eight days. On the other hand, samples B and C continue to change their TSI values, with sample C being the least kinetically stable.

However, one must take care: although sample C (the most polydisperse) did sediment the most and showed more pronounced destabilization kinetics, it is not possible to conclude that this sample is the worst when it comes to redispersibility. For that, redispersibility tests were also performed, and the results are shown in the supplementary material.

8. On-state yield stress and void fraction

To explain the increase in the yield stress under magnetic field, the Brouwers model [83] can be used. Considering the maximum packing fraction of each blend, ϕ_{\max} , one can define the void fraction φ as:

$$\varphi = 1 - \phi_{\max}. \quad (12)$$

As the data from the PSD are log-normally distributed, the log-normal void fraction (φ^{LN}), according to the Brouwers model, is given by:

$$\varphi^{\text{LN}} = \varphi_1 \sigma_g^{-\sqrt{2\pi}\beta(1-\varphi_1)} \quad (13)$$

where $\sigma_g = e^\sigma$ is the geometric standard deviation, φ_1 is the single-sized void fraction of the considered particle shape and β is the gradient in void fraction in the limit of a monosized system to a two-component system. It is worth noting that both φ_1 and β are physically defined constants and depend only on particle shape and the type of packing.

Rearranging equations (12) and (13), one can obtain the log-normal maximum packing fraction ϕ_{\max}^{LN} :

$$\phi_{\max}^{\text{LN}} = 1 - \varphi_1 \sigma_g^{-\sqrt{2\pi}\beta(1-\varphi_1)}. \quad (14)$$

It is also worth remembering that $\phi_{\max}^{\text{LN}} = \phi_{\max} \approx \phi_{\text{RCP}}$.

From equation (13), it is clear that the log-normal void fraction is strictly related to the standard deviation of the size distributions: by increasing the standard deviation (polydispersity) of the blends, the void fraction between the particles decreases, and the maximum packing fraction increases. This could be used to explain the performance gain of the on-state yield stress: a reduction in the void fraction could potentially strengthen the chain-like structures, increasing the yield stress and, therefore, increasing its resistance to break and flow.

To the best of our knowledge, the presented results are unprecedented and contradicts what has been commonly reported in the magnetorheology literature, so far. From the data, it can be seen that it is possible to optimize the main properties of a concentrated MRF (low off-state viscosity and high on-state yield stress) by increasing the polydispersity of the dispersed solid phase. Furthermore, these results point to the need for more studies on the influence of PSD in concentrated MRF and pave the way to the formulation of MRF with a more pronounced magnetorheological effect, further improving their applicability in mechanical systems.

This work aimed to demonstrate that polydispersity, described by size distributions of micrometric carbonyl iron particles with the same mode of $\sim 7 \mu\text{m}$, but different distribution widths, influences the maximum packing of these particles. In this context, three blends with the same volume fraction of 48.5 vol% were prepared; their difference was essentially only the width of the size histograms. Due to an increase in maximum packing, the shear viscosity in the

absence of a magnetic field is reduced by increasing polydispersity, as expected. In addition, contrary to what is often reported in the literature, we observed that this increase in polydispersity also increases the MR effect under an applied magnetic field induction $B_{\text{MRF}} \approx 0.57$ T with the gap filled with the MRF, at the CSS ramp test. Although it was not our objective to evaluate the effect of polydispersity on these MRF formulations' stability (or redispersibility), the results of these tests are also presented. Redispersibility as supplementary material. The redispersibility of the samples was measured after 30 d at rest under normal gravity (natural sedimentation). For more details on this essay, we recommend the reference Gomes de Sousa and Bombard [13]. Such tests unequivocally demonstrate that increasing polydispersity improves the redispersibility.

9. Conclusion

Among the many challenges encountered during the development of an MRF, the optimization of its main rheological properties (off-state viscosity and on-state yield stress) proves to be crucial and one of the several ways to do this is by adjusting the polydispersity. In this work, MRF whose size distributions showed the same mode ($\sim 7 \mu\text{m}$), but different degrees of polydispersity ($\alpha_A = 0.46$, $\alpha_B = 0.75$, and $\alpha_C = 1.44$) were prepared and investigated through experiments and simulations. By critically analyzing the data, it was observed that the widening of the size distributions caused an increase in the random close packing volume fractions (from 69.6% to 81.2% in the 1D case and from $67.3 \pm 0.2\%$ to $79.6 \pm 5.0\%$ in the 3D case) which, in turn, generates a decrease of about 90% (from 4.8 Pa.s to 0.5 Pa.s) in the off-state plastic viscosity and an increase of 40% (from 30.0 ± 0.5 kPa to 42 ± 2 kPa) in the on-state yield stress of the prepared fluids. The increase in the on-state yield stress could be assigned to a decrease in the void fractions, which strengthens the chain-like structures of the MRF. These results show that, contrary to what the literature often reports, it is possible to optimize the magnetorheological effect by increasing the polydispersity of the solid phase and point to the need for more studies on the influence of PSD in concentrated MRF. As a proposal for future works, further experiments are suggested, to investigate whether the observed trend applies to other smart materials, such as magnetorheological gels and electrorheological fluids, in addition to MRF with different materials and volume fractions. It is also suggested an evaluation of the effects of skewness and kurtosis on different size distributions of concentrated MRFs.

Data availability statement


All data that support the findings of this study are included within the article (and any supplementary files).

Acknowledgments

JGFM acknowledges Coordenação de Aperfeiçoamento de Pessoal de Nível Superior (CAPES) by his scholarship. He

also deeply thanks Emory University (Atlanta, GA) for the opportunity as well as the hospitality from Professor Eric Weeks' research group. This material is based upon work supported by the National Science Foundation under Grant Nos. CBET-1804186 (ERW). AJFB acknowledges: FAPEMIG Grants: APQ-01824-17 and PCI-00076-20 (Brazil), as well as Fundación Carolina (Spain) by the postdoc fellowship 'Movilidad de profesorado Brasil-España—call 2020'. The help of my colleague Professor Wilton S Dias with simulations is very appreciated. We also are in debt to Dr Farr for his kind help with his simulation code. We greatly appreciate the help and goodwill of the company DAFRATEC, SBC Brazil, Mr Dario Bonna Junior, and Mr. Claudemir José Papini, who very kindly allowed us to analyze our samples on the Turbiscan Lab. We thank and acknowledge the reviewers for their corrections.

ORCID iDs

Júlio Gabriel de Falco Manuel  <https://orcid.org/0000-0001-7514-2204>

Antonio José Faria Bombard  <https://orcid.org/0000-0002-8826-1197>

Eric R Weeks  <https://orcid.org/0000-0003-1503-3633>

References

- [1] Rabinow J 1948 The magnetic fluid clutch *Trans. Am. Inst. Electr. Eng.* **67** 1308–15
- [2] De Vicente J, Klingenberg D and Hidalgo-Alvarez R 2011 Magnetorheological fluids: a review *Soft Matter* **7** 3701–10
- [3] Olabi A G and Grunwald A 2007 Design and application of magneto-rheological fluid *Mater. Des.* **28** 2658–64
- [4] Tang H 2011 Particle size polydispersity of the rheological properties in magnetorheological fluids *Sci. China Phys. Mech. Astron.* **54** 1258–62
- [5] López-López M, Kuzhir P, Meunier A and Bossis G 2010 Synthesis and magnetorheology of suspensions of submicron-sized cobalt particles with tunable particle size *J. Phys.: Condens. Matter* **22** 324106
- [6] Carlson J D and Jolly M R 2000 MR fluid, foam and elastomer devices *Mechatronics* **10** 555–69
- [7] Cao J, Li J, Nie M, Zhu P, Zhao C, Zhang J, Xuan T, Xu J and Li B 2019 A novel surface polishing method and its fundamental performance in ultra-fine polishing of wafer *Int. J. Adv. Manuf. Technol.* **105** 2919–33
- [8] Jiang N, Sun S, Ouyang Y, Xu M, Li W and Zhang S 2016 A highly adaptive magnetorheological fluid robotic leg for efficient terrestrial locomotion *Smart Mater. Struct.* **25** 095019
- [9] El Wahed A and Balkhoyor L 2018 The performance of a smart ball-and-socket actuator applied to upper limb rehabilitation *J. Intell. Mater. Syst. Struct.* **29** 2811–22
- [10] El Wahed A 2020 A novel hydraulic actuation system utilizing magnetorheological fluids for single-port laparoscopic surgery applications *Materials* **13** 1380
- [11] Park B J, Fang F F and Choi H 2010 Magnetorheology: materials and application *Soft Matter* **6** 5246
- [12] Anupama A, Kumaran V and Sahoo B 2019 Effect of magnetic dipolar interactions and size dispersity on the origin of steady state magnetomechanical response in bidisperse Mn–Zn ferrite spherical particle based magnetorheological fluids *New J. Chem.* **43** 9969–79

- [13] Gomes de Sousa S R and Bombard A J F 2019 Redispersibility and its relevance in the formulation of magnetorheological fluids *Magnetorheological Materials and Their Applications* ed C Seung-Bok and L Weihua (London: IET—The Institution of Engineering and Technology) pp 1–18
- [14] Guerrero-Sanchez C, Lara-Ceniceros T, Jimenez-Regalado E, Raşa M and Schubert U 2007 Magnetorheological fluids based on ionic liquids *Adv. Mater.* **19** 1740–7
- [15] Shah K and Choi S 2014 The field-dependent rheological properties of magnetorheological fluids featuring plate-like iron particles *Front. Mater.* **1** 1–6
- [16] Morillas J and de Vicente J 2020 Magnetorheology: a review *Soft Matter* **16** 9614–42
- [17] Pednekar S, Chun J and Morris J 2018 Bidisperse and polydisperse suspension rheology at large solid fraction *J. Rheol.* **62** 513–26
- [18] Farris R 1968 Prediction of the viscosity of multimodal suspensions from unimodal viscosity data *Trans. Soc. Rheol.* **12** 281–301
- [19] Ota M and Miyamoto T 1994 Optimum particle size distribution of an electrorheological fluid *J. Appl. Phys.* **76** 5528–32
- [20] Lemaire E, Meunier A, Bossis G, Liu J, Felt D, Bashtovoi P and Matussevitch N 1995 Influence of the particle size on the rheology of magnetorheological fluids *J. Rheol.* **39** 1011–20
- [21] Ramos J, Klingenberg D, Hidalgo-Álvarez R and de Vicente J 2011 Steady shear magnetorheology of inverse ferrofluids *J. Rheol.* **55** 127–52
- [22] Wang Z, Zhi-fang L and Rui-bao T 1997 Influence of the size distribution of particles on the viscous property of an electrorheological fluid *Chin. Phys. Lett.* **14** 151–4
- [23] Mori Y, Tsunamoto T and Nakayama H 1999 Computer simulation of electrorheological fluids in the binary system of particle size *Int. J. Mod. Phys. B* **13** 1822–7
- [24] de Gans B, Duin N, van den Ende D and Mellema J 2000 The influence of particle size on the magnetorheological properties of an inverse ferrofluid *J. Chem. Phys.* **113** 2032–42
- [25] See H, Kawai A and Ikazaki F 2002 The effect of mixing particles of different size on the electrorheological response under steady shear flow *Rheol. Acta* **41** 55–60
- [26] Trendler A and Böse H 2005 Influence of particle size on the rheological properties of magnetorheological suspensions *Int. J. Mod. Phys. B* **19** 1416–22
- [27] Saldivar-Guerrero R, Richter R, Rehberg I, Aksel N, Heymann L and Rodriguez-Fernández O 2006 Viscoelasticity of mono- and polydisperse inverse ferrofluids *J. Chem. Phys.* **125** 084907
- [28] Kantorovich S 2003 Electronic structure and magnetic properties of GdM₂ compounds *J. Magn. Magn. Mater.* **258–259** 471–3
- [29] Wang Z and Holm C 2003 Structure and magnetic properties of polydisperse ferrofluids: a molecular dynamics study *Phys. Rev. E* **68** 041401
- [30] Tao R 2007 The physical mechanism to reduce viscosity of liquid suspensions *Int. J. Mod. Phys. B* **21** 4767–73
- [31] Ekwebelam C and See H 2007 Using oscillatory shear to probe the effects of bidispersity in inverse ferrofluids *Korea Aust. Rheol. J.* **19** 35–42
- [32] Chiriac H and Stoian G 2009 Influence of the particles size and size distribution on the magnetorheological fluids Properties *IEEE Trans. Magn.* **45** 4049–51
- [33] Segovia-Gutiérrez J, de Vicente J, Hidalgo-Álvarez R and Puertas A 2013 Brownian dynamics simulations in magnetorheology and comparison with experiments *Soft Matter* **9** 6970
- [34] Sherman S and Wereley N 2013 Effect of particle size distribution on chain structures in magnetorheological fluids *IEEE Trans. Magn.* **49** 3430–3
- [35] Sarkar C and Hirani H 2015 Effect of particle size on shear stress of magnetorheological fluids *Smart Sci.* **3** 65–73
- [36] Fernández-Toledano J, Ruiz-López J, Hidalgo-Álvarez R and de Vicente J 2015 Simulations of polydisperse magnetorheological fluids: a structural and kinetic investigation *J. Rheol.* **59** 475–98
- [37] Schulz G 1939 Über die kinetik der kettenpolymerisationen. V *Z. Phys. Chem.* **43B** 25–46
- [38] Ruiz-López J, Wang Z, Fernández-Toledano J, Hidalgo-Álvarez R and de Vicente J 2016 Start-up rheometry of highly polydisperse magnetorheological fluids: experiments and simulations *Rheol. Acta* **55** 245–56
- [39] Foister R 1997 Magnetorheological fluids *United States Patent* 5,667,715
- [40] Allen T 1997 *Particle Size Measurement: Powder Sampling and Particle Size Measurement* 5th edn (London: Chapman & Hall)
- [41] Yu A and Standish N 1990 A study of particle size distributions *Powder Technol.* **62** 101–18
- [42] Limpert E, Stahel W and Abbt M 2001 Log-normal distributions across the sciences: keys and clues *Biosci.* **51** 341–252
- [43] Ferrari J, Castilhos F, Araújo P and Sayer C 2016 Modeling particle size distribution in heterogeneous polymerization systems using multimodal lognormal function *Braz. J. Chem. Eng.* **33** 469–78
- [44] Brosseau L, Fang C, Snyder C and Cohen B 1992 Particle size distribution of automobile paint sprays *J. Occup. Environ. Hyg.* **7** 607–12
- [45] Brittain H G 2001 Solid-state analysis *Handbook of Modern Pharmaceutical Analysis* ed S Ahuja and S Scypinski (Amsterdam: Elsevier) pp 57–84
- [46] Desmond K W and Weeks E R 2014 Influence of particle size distribution on random close packing of spheres *Phys. Rev. E* **90** 022204
- [47] Polakowski C, Sochan A, Bieganski A, Ryzak M, Földényi R and Tóth J 2014 Influence of the sand particle shape on particle size distribution measured by laser diffraction method *Int. Agrophys.* **28** 195–200
- [48] Adi H, Larson I and Stewart P 2007 Use of milling and wet sieving to produce narrow particle size distributions of lactose monohydrate in the sub-sieve range *Powder Technol.* **179** 95–99
- [49] Hopkins K and Weeks D 1990 Tests for normality and measures of skewness and kurtosis: their place in research reporting *Educ. Psychol. Meas.* **50** 717–29
- [50] Blanca M, Arnau J, López-Montiel D, Bono R and Bendayan R 2013 Skewness and kurtosis in real data samples *Methodology* **9** 78–84
- [51] DeCarlo L 1997 On the meaning and use of kurtosis *Psychol. Methods* **2** 292–307
- [52] Peacock B, Hastings N, Evans M and Forbes C 2011 *Statistical Distributions* 4th edn (Hoboken: John Wiley & Sons, Inc)
- [53] Crow E and Shimizu K 1988 *Lognormal Distributions: Theory and Applications* (New York: Marcel Dekker)
- [54] Sinharay S 2010 Continuous probability distributions *International Encyclopedia of Education* 3rd edn, ed P Peterson, E Baker and B McGaw (Amsterdam: Elsevier) pp 98–102
- [55] Kintz K and Forehand T 2005 MR fluid for increasing the output of a magnetorheological fluid damper *United States Patent* 6,886,819 B2
- [56] Ierardi R and Bombard A 2009 Off-state viscosity and yield stress optimization of magneto-rheological fluids: a mixture

- design of experiments approach *J. Phys.: Conf. Ser.* **149** 012037
- [57] Oetter G, Laun M, Pfister J, Lochtmann R, Lippert G and Maas H 2011 Magnetorheological liquid *United States Patent* 7,959,822 B2
- [58] Kumar Kariganaur A, Kumar H and Arun M 2022 Effect of temperature on sedimentation stability and flow characteristics of magnetorheological fluids with damper as the performance analyser *J. Magn. Magn. Mater.* **555** 169342
- [59] Wang G, Zhao D, Ma Y, Zhang Z, Che H, Mu J, Zhang X, Tong Y and Dong X 2017 Synthesis of calcium ferrite nanocrystal clusters for magnetorheological fluid with enhanced sedimentation stability *Powder Technol.* **322** 47–53
- [60] Mrlik M, Sedlacik M, Pavlinek V, Bazant P, Saha P, Peer P and Filip P 2012 Synthesis and magnetorheological characteristics of ribbon-like, polypyrrole-coated carbonyl iron suspensions under oscillatory shear *J. Appl. Polym. Sci.* **128** 2977–82
- [61] Cheng H, Wang J, Zhang Q and Wereley N 2009 Preparation of composite magnetic particles and aqueous magnetorheological fluids *Smart Mater. Struct.* **18** 085009
- [62] Legay-Désesquelles F, Prunet-Foch B and Vignes-Adler M 1993 Sedimentation of metallic particles in oils and emulsions *Colloids Surf. A* **75** 75–83
- [63] Farr R and Groot R 2009 Close packing density of polydisperse hard spheres *J. Chem. Phys.* **131** 244104
- [64] Farr R 2013 Random close packing fractions of lognormal distributions of hard spheres *Powder Technol.* **245** 28–34
- [65] Xu N, Blawdziewicz J and O'Hern C 2005 Random close packing revisited: ways to pack frictionless disks *Phys. Rev. E* **71** 061306
- [66] Desmond K W and Weeks E R 2009 Random close packing of disks and spheres in confined geometries *Phys. Rev. E* **80** 051305
- [67] Newman M 2005 Power laws, Pareto distributions and Zipf's law *Contemp. Phys.* **46** 323–51
- [68] Yefimov N and Neikov O 2019 Powder characterization and testing *Handbook of Non-Ferrous Metal Powders: Technologies and Applications* 2nd edn, ed N Yefimov, O Neikov and S Naboychenko (Amsterdam: Elsevier) pp 3–62
- [69] Kintz K and Forehand T 2006 MR fluid for increasing the output of a magnetorheological fluid device *United States Patent* 7,087,184 B2
- [70] Macosko C 1994 *Rheology: Principles, Measurements, and Applications* (New York: Wiley-VCH)
- [71] Krieger I and Dougherty T 1959 A mechanism for non-Newtonian flow in suspensions of rigid spheres *Trans. Soc. Rheol.* **3** 137–52
- [72] Mezger T 2014 *The Rheology Handbook* 4th edn (Hanover: Vincentz Network)
- [73] Coussot P 2012 Introduction to the rheology of complex fluids *Understanding the Rheology of Concrete: A Volume in Woodhead Publishing Series in Civil and Structural Engineering* ed N Roussel (Cambridge: Woodhead Publishing) pp 3–22
- [74] Koka V, Papachristodoulou G and Trass O 1985 Settling stability of coal slurries prepared by wet grinding in the Szego mill *Can. J. Chem. Eng.* **63** 585–90
- [75] Morillas J, Bombard A and de Vicente J 2015 Preparation and characterization of magnetorheological fluids by dispersion of carbonyl iron microparticles in PAO/1-octanol *Smart Mater. Struct.* **25** 015023
- [76] Kesavan S 1986 Formulation of stable coal-methanol suspensions using coal liquids *Fuel Sci. Technol. Int.* **4** 191–206
- [77] Luo M, Qi X, Ren T, Huang Y, Keller A, Wang H, Wu B, Jin H and Li F 2017 Heteroaggregation of CeO₂ and TiO₂ engineered nanoparticles in the aqueous phase: application of turbiscan stability index and fluorescence excitation-emission matrix (EEM) spectra *Colloids Surf. A* **533** 9–19
- [78] Mengual O, Meunier G, Cayré I, Puech K and Snabre P 1999 Turbiscan MA 2000: multiple light scattering measurement for concentrated emulsion and suspension instability analysis *Talanta* **50** 445–56
- [79] Kim H and Choi H 2022 Enhanced magnetorheological response of carbonyl iron suspension with added ZnFe₂O₄ particles *IEEE Trans. Magn.* **58** 1–5
- [80] Dong Y, Esmailnezhad E and Choi H 2021 Core-shell structured magnetite-poly(diphenylamine) microspheres and their tunable dual response under magnetic and electric fields *Langmuir* **37** 2298–311
- [81] Cvek M, Mrlik M, Moucka R and Sedlacik M 2018 A systematic study of the overall influence of carbon allotrope additives on performance, stability and redispersibility of magnetorheological fluids *Colloids Surf. A* **543** 83–92
- [82] Formulation 2018 User Guide *Turbiscan Lab User Guide* (Toulouse: Formulation)
- [83] Brouwers H 2014 Packing fraction of particles with lognormal size distribution *Phys. Rev. E* **89** 052211